Experimental Implementation of Extended Multivariable PPF Control on an Active Structure

S. O. Reza Moheimani, *Senior Member, IEEE*, Benjamin J. G. Vautier, and Bharath Bhikkaji

***Abstract*—This paper reports experimental implementation of an extended positive position feedback (PPF) controller on an active structure consisting of a cantilevered beam with bonded collocated piezoelectric actuators and sensors. Stability conditions for PPF control are rederived to allow for a feed-through term in the model of the structure. This feed-through term is needed to ensure that the system's in-bandwidth zeros are captured with reasonable accuracy. The set of stabilizing PPF controllers is shown to be a convex set characterized by a set of linear matrix inequalities. A number of multivariable PPF controllers are designed and successfully implemented on the structure.**

***Index Terms*—Flexible structures, multivariable systems, piezoelectric transducers, positive position feedback (PPF), vibration control.**

I. Introduction

A major difficulty in controlling flexible structures is due to the fact that they are distributed parameter systems. Consequently, these structures have a very large amount of vibration modes and their transfer functions contain many poles close to the $j\omega$ axis. These systems are generally difficult to control.

In most cases, a small number of in-bandwidth modes of the structure are required to be controlled, and it is possible that some in-bandwidth modes are not targeted to be controlled at all. The presence of uncontrolled modes can lead to the problem of spillover [1], [2]. That is, the control energy is channeled to the residual modes of the system and this process may destabilize the closed-loop system. In particular, the spillover effect is of major concern at higher frequencies where obtaining a precise model of the structure is rather difficult.

One approach to overcome the spillover effect is based on using collocated sensors and actuators. To this end, a number of control design techniques have been proposed that guarantee unconditional closed-loop stability and can add sufficient damping to the structure. Velocity feedback [3], [4] and resonant controllers [5] are two examples of such controllers.

Positive position feedback as proposed by Caughey *et al.* [6], [7] is an alternative control design technique for flexible structures with collocated sensors and actuators, which is insensitive to the spillover effect. The positive position feedback (PPF) controller does not guarantee unconditional stability of the closed-loop system; however, it does guarantee stability in presence of uncontrolled in-bandwidth modes, and it has the additional property that it rolls off quickly at higher frequencies.

One of the shortcomings of PPF as proposed in [6] and [7] is that the effect of out-of-bandwidth modes on the dynamics of the controlled modes is ignored. Dynamics of distributed parameter systems such as flexible structures are governed by partial differential equations (PDEs) [8]. These PDEs are discretized to obtain a lumped model of the system. Consequently, the transfer functions of flexible structures consist of a very large number of highly resonant terms. Out-of-bandwidth terms are often removed from the model to simplify the task of designing a controller. This introduces an error that manifests itself by perturbing in-bandwidth zeros of the system, which could be detrimental to the closed-loop stability of the controlled system [9]. In particular, when the actuators and sensors are collocated, this effect is exacerbated. This problem can be alleviated by adding a feed-through term to the truncated model of the system [9], [10]. Therefore, the stability conditions for the PPF controller need to be rederived accordingly.

In this paper, we derive stability conditions for PPF controllers when the underlying structure model contains a feed-through term. We also design a number of multivariable PPF controllers for a test structure consisting of a cantilevered beam and several bonded piezoelectric actuators and sensors. Although a drastic simplification of a real structure, a thin beam is dynamically well understood, retains the important characteristics of the real structure, and is an ideal experimental testbed to evaluate performance of the PPF controllers.

This paper continues as follows. Section II introduces the class of systems under investigation in this work. Section III discusses two controllers that are guaranteed to be closed-loop stable, namely the velocity controller and resonant controllers. Section IV is concerned with deriving stability conditions for PPF controlled systems. It is also illustrated that the set of stabilizing PPF controllers is a convex set, characterized by a number of linear matrix inequalities. Section V contains details of the experimental setup used to evaluate performance of PPF controllers. Section VI describes how a model of the system suitable for control design purposes is identified. Section VII describes a number of possible performance criteria for PPF controllers and explains how an appropriate set of initial conditions can be determined to start the resulting nonlinear optimization problems. Our experimental results and simulations are contained in the same section. Finally, Section VIII concludes the paper.

Manuscript received March 4, 2005. Manuscript received in final form December 13, 2005. Recommended by Associate Editor R. Erwin. This work was supported by the Australian Research Council.

The authors are with the School of Electrical Engineering and Computer Science, The University of Newcastle, Newcastle, NSW 2308, Australia (e-mail: reza@ee.newcastle.edu.au).

Digital Object Identifier 10.1109/TCST.2006.872532

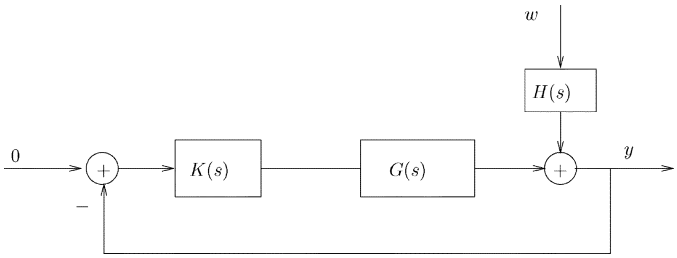

Fig. 1. Feedback control system associated with a flexible structure with collocated actuator/sensor pairs, and subject to disturbance w.

II. Resonant Systems

In this paper, we are concerned with designing high-performance feedback controllers for multivariable resonant systems of the form

$$G(s) = \sum_{i=1}^{M} \frac{\psi_i \psi_i'}{s^2 + 2\zeta_i \omega_i s + \omega_i^2} \tag{1}$$

where ψ_i is an $m \times 1$ vector, and $M \to \infty$. In practice, however, the integer M is finite, but possibly a very large number which represents the number of modes that sufficiently describe the elastic properties of the structure under excitation [4], [11]. Furthermore, the structure could be subject to disturbances represented by w, whose effect may be captured by a transfer function $H(s)$. This could represent point forces, distributed forces (such as a wind gust), or torques acting on the structure. The transfer function matrix relating the disturbance vector w to the measured outputs can be represented as

$$H(s) = \sum_{i=1}^{M} \frac{\psi_i \gamma_i'}{s^2 + 2\zeta_i \omega_i s + \omega_i^2} \tag{2}$$

where γ_i is a $\ell \times 1$ matrix, assuming there are ℓ disturbances acting on the structure.

For the soft–input soft–output (SISO) case, i.e., when $G(s)$ represents the transfer function associated with only one collocated actuator/sensor pair, this system is known to possess interesting properties [12]. In particular, it is known that the system is minimum phase, and furthermore, poles and zeros of the system interlace. This ensures that the phase of the collocated transfer function will be within the 0° to -180° range.

Given the highly resonant nature of flexible structures, it is natural to investigate ways of adding damping to the structure. One way of adding damping to the structure is to use a feedback controller $K(s)$, as demonstrated in Fig. 1.

III. Resonant Controllers

The structure of the collocated system, as expressed by (1), allows for the design of feedback controllers, with specific structures, that guarantee unconditional stability of the closed-loop system. Such controllers are of interest due to their ability to avoid closed-loop instabilities arising from the spill-over effect [2]. A possible controller that guarantees unconditional closed-loop stability of the collocated system is the velocity feedback controller. This feedback controller is defined as [1], [2], [13]

$$K(s) = \gamma' \gamma s. \tag{3}$$

The closed-loop stability of (1) under (3) can be verified in a number of ways. In the SISO case, this can be explained graphically. Being a collocated transfer function, phase of $G_{vv}(s)$ is between 0° and -180°. This, along with the fixed 90° phase of the differentiator and the negative feedback gain of -1, ensures that Nyquist plot of $sG(s)$ will not circle $-1 + \mathrm{j}0$ point in the complex plane.

Although velocity feedback allows for spillover, existence of spillover does not destabilize the closed-loop system. This is a very interesting property. However, despite its appealing stability properties, velocity feedback as described by (3) is of little use in many applications. The main problem is due to the fact that one would need to implement a differentiator, which is not possible given the large bandwidth of the system. Some extra dynamics would have to be added to the compensator to make sure that it would rolloff at higher frequencies. These extra dynamics have the potential to destabilize the closed-loop system due to the high-bandwidth nature of the underlying system.

Another problem with velocity feedback, which is perhaps of a greater concern, is the high-control effort at all frequencies. For vibration damping purposes, the control effort should ideally be restricted to regions around resonance frequencies of the base structure. This calls for different classes of controllers that are capable of providing sufficient damping and have good stability properties. Resonant controllers satisfy these conditions. These controllers approximate a differentiator at a narrow bandwidth around the resonance frequencies of the structure.

Two possible resonant controllers are

$$K^{\alpha}(s) = \sum_{i=1}^{\tilde{N}} \frac{\alpha_i \alpha_i' s^2}{s^2 + 2d_i \tilde{\omega}_i s + \tilde{\omega}_i^2} \tag{4}$$

and

$$K^{\beta}(s) = \sum_{i=1}^{\tilde{N}} \frac{\beta_i \beta_i' s(s + 2d_i \tilde{\omega}_i)}{s^2 + 2d_i \tilde{\omega}_i s + \tilde{\omega}_i^2} \tag{5}$$

where, typically, $\tilde{N} \ll M$. Note that both α_i and β_i are $m \times 1$ vectors.

The typical feedback control problem associated with system (1) and a resonant controller K is illustrated in Fig. 1. Here, y is the output of the system as measured by a sensor, while W is the vector of disturbances acting on the structure. The purpose of the controller is to add damping to the structure, hence reducing the effect of disturbances on the structure. This is done by shifting closed-loop poles of the system deeper into the left half of the complex plane.

Closed-loop stability of the multivariable collocated system (1) under (4) and (5) can be proved in a number of ways. Although we do not intend to prove the closed-loop stability of these systems here, we point the reader to [5] for a thorough proof.

One of the issues with resonant controllers is their limited performance in terms of adding damping to the structure. Positive position feedback controllers can provide higher levels of damping and have good stability properties.

IV. Positive Position Feedback Control

One of the difficulties associated with implementation of resonant controllers introduced in the previous section is the fact that frequency responses of (4) and (5) do not rolloff at higher frequencies. Although, under ideal assumptions, the closed-loop stability of collocated system (1) under (4) and (5) is guaranteed, in real world applications, due to issues such as phase contributions of the antialiasing filters, etc., the existence of out-of-bandwidth dynamics may destabilize the closed-loop system. Another issue is the limited performance one could expect from a resonant controller. The passive nature [14], [15] of the controller means that there will be a limit on how much damping it can add to the structure. It is, therefore, of interest to have a high-performance controller which possesses similar structure to (4) and (5), but whose frequency response rolls off at higher frequencies. Positive position feedback, proposed by Caughey *et al.* [6], [7] has such properties.

For a system of the form (1), a positive position feedback controller is defined as

$$K_{pp}(s)=\sum_{i=1}^{\tilde{N}}\frac{-\gamma_i\gamma_i'}{s^2+2\delta_i\tilde{\omega}_i s+\tilde{\omega}_i^2} \tag{6}$$

where $\gamma_i\in\mathbf{R}^{m\times 1}$ for $i=1,2,\ldots,\tilde{N}$.

As illustrated in Fig. 1, due to the existence of the negative sign in all terms of (6), the overall system resembles a positive feedback loop. Also, the transfer function matrix (1) is similar to that of the force to displacement transfer function matrix associated with a flexible structure, hence, the terminology positive position feedback.

An important property of PPF controllers is that to suppress one vibration mode requires only one second-order term, as articulated in (6). Consequently, one can choose the modes, within a specific bandwidth, that are to be controlled and construct the necessary controller. This ensures that dimensions of the controller remain small, which is beneficial when the controller is being implemented. In the experimental part of this paper we will illustrate that despite their simple structure, the PPF controllers are highly efficient in damping structural vibrations and are capable of maintaining performance in presence of uncertainty in the structural dynamics of the system.

To derive stability conditions for this control loop, the series in (1) is first truncated by keeping the first N modes ($N<M$) that lie within the bandwidth of interest, and then incorporating the effect of truncated modes by adding a feed-through term to the truncated model. That is, to approximate (1) by

$$G^N(s)=\sum_{i=1}^{N}\frac{\psi_i\psi_i'}{s^2+2\zeta_i\omega_i s+\omega_i^2}+D. \tag{7}$$

The addition of this feed-through term to the truncated model is quite important, if the truncation is not to substantially alter open-loop zeros of the system. Although the truncation does not perturb open-loop poles of the system, it has the potential to significantly move the open-loop zeros, particularly when the actuators and sensors are collocated. Consequently, if a feedback controller is designed for the truncated model, and then implemented on the real system, the performance and stability of the closed-loop system could be adversely affected. This issue has been well known to the aeroelasticity community and has been referred to as the mode acceleration method [16]. This area has been recently revisited, and a number of optimal choices for the feed-through term D have been suggested [9], [10], [17], [18].

Currently available PPF techniques do not allow for a feed-through term in the plant model. In our experience, however, it is essential to include this in the design phase, if the implemented controller is to perform in a satisfactory manner. Closed-loop performance of controlled system is highly dependent on open-loop zeros of the plant [19]. Inclusion of a feed-through term in the model ensures that closed-loop performance of the controller, once implemented, is in close agreement with theoretical predictions.

To derive stability of (7) under (6), the following theorem is needed.

Theorem 1: Consider the following second-order multivariable dynamical system:

$$\ddot{x}(t)+\mathcal{D}\dot{x}(t)+\mathcal{K}x(t)=0 \tag{8}$$

where $\mathcal{D},\mathcal{K}\in\mathbf{R}^{N\times N}$ and $x\in\mathbf{R}^{N\times 1}$. Furthermore, assume that $\mathcal{D}=\mathcal{D}'>0$. Then, (8) is exponentially stable if and only if $\mathcal{K}=\mathcal{K}'>0$.

Proof: See [6] for a proof. ∎

The following theorem gives the necessary and sufficient conditions for closed-loop stability under positive position feedback. First, we need to make the following definitions:

$$Z=\begin{bmatrix}\zeta_1 & & & \\ & \zeta_2 & & \\ & & \ddots & \\ & & & \zeta_N\end{bmatrix}\quad \Omega=\begin{bmatrix}\omega_1 & & & \\ & \omega_2 & & \\ & & \ddots & \\ & & & \omega_N\end{bmatrix}$$

$$\Psi=\begin{bmatrix}\psi_1 & \psi_2 & \ldots & \psi_N\end{bmatrix}$$

and

$$\Delta=\begin{bmatrix}\delta_1 & & & \\ & \delta_2 & & \\ & & \ddots & \\ & & & \delta_{\tilde{N}}\end{bmatrix}\quad \tilde{\Omega}=\begin{bmatrix}\tilde{\omega}_1 & & & \\ & \tilde{\omega}_2 & & \\ & & \ddots & \\ & & & \tilde{\omega}_{\tilde{N}}\end{bmatrix}$$

$$\Gamma=\begin{bmatrix}\gamma_1 & \gamma_2 & \ldots & \gamma_{\tilde{N}}\end{bmatrix}.$$

Furthermore, we assume that

$$\Delta>0. \tag{9}$$

Theorem 2: The negative feedback connection of (7) and (6) with (9) is exponentially stable if and only if

$$\tilde{\Omega}^2-\Gamma' D\Gamma>0 \tag{10}$$

and

$$\Omega^2-\Psi'\Gamma(\tilde{\Omega}^2-\Gamma' D\Gamma)^{-1}\Gamma'\Psi>0. \tag{11}$$

Proof: Using the above notation, (6) and (7) can be represented in state-space form as

$$\ddot{x}(t)+2Z\Omega\dot{x}(t)+\Omega^2x(t)=\Psi'u(t) \tag{12}$$

$$y(t)=\Psi x(t)+Du(t) \tag{13}$$

and

$$\ddot{\tilde{x}}(t)+2\Delta\tilde{\Omega}\dot{\tilde{x}}(t)+\tilde{\Omega}^2\tilde{x}(t)=\Gamma' y(t) \tag{14}$$

$$u(t)=\Gamma\tilde{x}(t) \tag{15}$$

where $x\in\mathbf{R}^{N\times 1}$, $\tilde{x}\in\mathbf{R}^{\tilde{N}\times 1}$, $u\in\mathbf{R}^{m\times 1}$, and $y\in\mathbf{R}^{m\times 1}$.

The closed-loop system can then be written as

$$\begin{bmatrix}\ddot{x}(t)\\ \ddot{\tilde{x}}(t)\end{bmatrix}+\begin{bmatrix}2Z\Omega & 0\\ 0 & 2\Delta\tilde{\Omega}\end{bmatrix}\begin{bmatrix}\dot{x}(t)\\ \dot{\tilde{x}}(t)\end{bmatrix}+\begin{bmatrix}\Omega^2 & -\Psi'\Gamma\\ -\Gamma'\Psi & \tilde{\Omega}^2-\Gamma'D\Gamma\end{bmatrix}\begin{bmatrix}x(t)\\ \tilde{x}(t)\end{bmatrix}=\begin{bmatrix}0\\ 0\end{bmatrix}. \quad (16)$$

Clearly

$$\begin{bmatrix}2Z\Omega & 0\\ 0 & 2\Delta\tilde{\Omega}\end{bmatrix}>0.$$

Therefore, according to Theorem 1, the closed-loop system is stable if and only if

$$\begin{bmatrix}\Omega^2 & -\Psi'\Gamma\\ -\Gamma'\Psi & \tilde{\Omega}^2-\Gamma'D\Gamma\end{bmatrix}>0. \quad (17)$$

The Schur complement [20] implies that this inequality holds if and only if

$$\tilde{\Omega}^2-\Gamma'D\Gamma>0$$

and

$$\Omega^2-\Psi'\Gamma(\tilde{\Omega}^2-\Gamma'D\Gamma)^{-1}\Gamma'\Psi>0$$

which proves the theorem. ■

It should be pointed out that the stability condition (10), (11) can be represented by a linear matrix inequality in variables Δ, $\tilde{\Omega}^2$ and Ψ, by applying Schur complement as indicated in the following lemma.

Lemma 1: The set of positive position feedback controllers is a convex set characterized by the following linear matrix inequalities:

$$\Delta>0 \quad (18)$$

and

$$\begin{bmatrix}\Omega^2 & -\Psi'\Gamma & 0\\ -\Gamma'\Psi & \tilde{\Omega}^2 & \Gamma'\\ 0 & \Gamma & D^{-1}\end{bmatrix}>0. \quad (19)$$

Proof: This can be proved using Schur complement as follows:

$$\begin{bmatrix}\Omega^2 & -\Psi'\Gamma\\ -\Gamma'\Psi & \tilde{\Omega}^2-\Gamma'D\Gamma\end{bmatrix}>0$$

$$\Updownarrow$$

$$\begin{bmatrix}\Omega^2 & -\Psi'\Gamma\\ -\Gamma'\Psi & \tilde{\Omega}^2\end{bmatrix}-\begin{bmatrix}0\\ \Gamma'\end{bmatrix}D\begin{bmatrix}0 & \Gamma\end{bmatrix}>0$$

$$\Updownarrow$$

$$\begin{bmatrix}\omega^2 & -\Psi'\Gamma & 0\\ -\Gamma'\Psi & \tilde{\Omega}^2 & \Gamma'\\ 0 & \Gamma & D^{-1}\end{bmatrix}>0.$$

■

An implication of Lemma 1 is that all admissible positive position feedback controllers must be stable, as dictated by condition (18).

Positive position feedback controllers are generally capable of ensuring higher levels of performance compared to resonant controllers (4) and (5). However, in making a comparison, one has to be careful about the assumptions made in proving stability of the closed-loop systems associated with two different classes of controllers. To prove stability under feedback controllers (4) and (5), no simplifying assumption about the system needs to be made. Indeed, it can be proved that stability of the full-order system is guaranteed under these two controllers. However, to obtain stability conditions for the positive position feedback controller, we need to assume that a truncated model of the system with only N modes adequately represents the dynamics of the system within the bandwidth of interest. Although, from a mathematical point of view, this may present a problem, in most realistic applications in which sensors and actuators have limited bandwidths, this assumption is unlikely to be of concern. Indeed, many applications for positive position feedback control have been reported in the literature. To this end, the reader is referred to [21]–[29] and references therein.

To conclude this section we once more emphasize that the stability condition (10), (11) does allow for a nonzero feed-through term in the model of the system (7). As argued in [9], inclusion of a feed-through term in the model of a flexible structure may be essential, particularly when sensors and actuators are collocated. It should be noted that this analysis is missing from the original work of Fanson and Caughy [7]. Nevertheless, the stability condition reported in [7] can be derived from (10) and (11) by setting D to zero.

V. Experimental Setup

All discussions on resonant systems so far were based on analytic models (1), (2), and (7). The model structures of the resonant controllers and PPF controllers [see (4)–(6)] strongly resemble the system model structures (1), (2), and (7). Here, a cantilever beam representing a physical resonant system is considered. This beam, which is clamped at one end and free at the other end, is susceptible to high amplitude vibrations when disturbed. In what follows, a PPF controller will be designed to damp these highly resonant vibration modes of the beam. It is worth noting that the cantilever beams of the type to be used here are known to have models of the form (1), (2), and (7) (see [30]), and resonant controllers designed for them are known to have damped the vibrations to a reasonable extent (see [31] and [5]).

In this section, a description of the experimental setup meant for both modeling and control of the beam is presented. This setup will remain the same for all the experiments to be performed on the beam.

As mentioned above, the cantilever beam is clamped at one end and free at the other. Two pairs of piezoelectric patches are attached to this beam, one pair located close to the clamped end and the other pair located close to the free end of the beam. For each pair, one piezoelectric patch will be used as an actuator (where input signals are applied) and the other patch will act as a sensor (where output signals are recorded). Another solitary piezoelectric patch is attached to the center of the beam and will be driven by a voltage source w. This voltage w represents the disturbance on the beam. See Figs. 2 and 3 for a schematic beam setup and an actual picture of the beam, respectively.

Not surprisingly, the mechanical properties (including the damping and the resonance frequencies) will depend on the dimensions and material properties of the beam and the piezo patches. In Fig. 4 and Tables I and II, the dimensions of the beam setup and the material properties of the beam and the piezos are given.

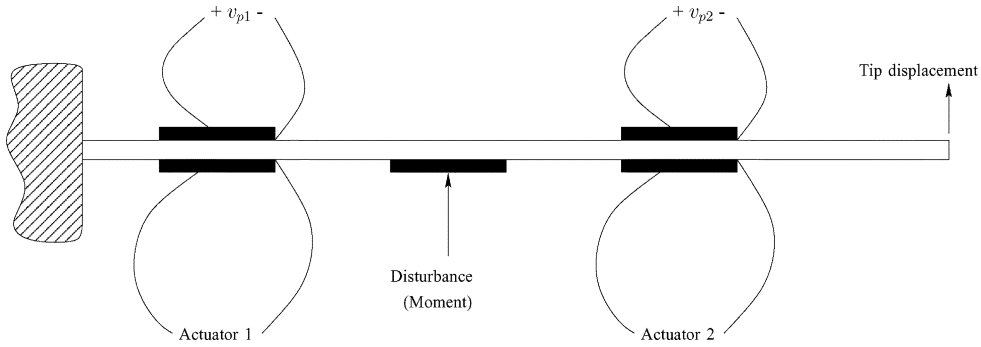

Fig. 2. Beam layout as used in the experiments.

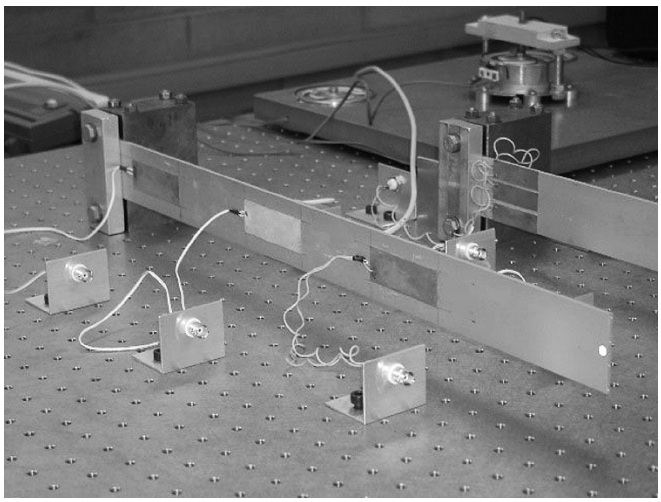

Fig. 3. Picture of the cantilever beam.

VI. System Identification

In order to obtain a model for the beam, the experimental setup is treated as a three-input three-output multivariable system (see Fig. 5). The inputs (v_1 and v_2) in Fig. 5 are the voltages applied to the actuators of the collocated piezo patches and the outputs v_{p1} and v_{p2} are the voltages induced at the corresponding sensors. The third input w is the disturbance on the beam and the output $y_{\rm tip}$ is the displacement of the the tip of the beam. To be precise, $y_{\rm tip}$ is the displacement of the top vertex point of the beam at the free end.

Since the system is modeled as a three-input three-output system, the frequency response function (FRF) $G(\mathrm{i}\omega)$ is a 3×3 matrix with each element $G_{ij}(\mathrm{i}\omega)$, i,j =1, 2, and 3, corresponding to a particular combination of the input and the output, i.e.,

$$G_{ij}(\mathrm{i}\omega)=G_{y_iu_j}=\frac{Y_i(\mathrm{i}\omega)}{U_j(\mathrm{i}\omega)} \tag{20}$$

where $y_1=y_{\rm tip}$, $y_2=v_{p1}$, and $y_3=v_{p2}$ and $u_1=w$, $u_2=v_1$, and $u_3=v_2$. $Y_i(\mathrm{i}\omega)$ and $U_j(\mathrm{i}\omega)$ are the Fourier transforms of y_i and u_j, respectively. These FRFs are determined (nonparametrically) by applying a sinusoidal chirp of varying frequency (from 5 to 250 Hz) to the piezoelectric actuators (including the central patch corresponding to the disturbance term w) and measuring the corresponding output signals $y_{\rm tip}$, v_{p1}, and v_{p2}. The inputs are generated using a standard HP signal generator and the output signals $y_{\rm tip}$, v_{p1}, and v_{p2} were measured using a Polytec laser scanning vibrometer (PSV-300). The vibrometer PSV-300 also includes a software which processes the input–output data to give a nonparametric $G(\mathrm{i}\omega)$. A nonparametric $G(\mathrm{i}\omega)$ refers to the case where values of $G(\mathrm{i}\omega)$ are calculated at certain frequency points ω_k, $k=1,2,\dots M$, and interpolated in the intervals $\omega_k\le\omega\le\omega_{k+1}$.

In Fig. 6, the nonparametric FRFs $G_{ij}(\mathrm{i}\omega)$, i,j =1, 2, and 3 are plotted. It is apparent from the plots that all the FRFs have three resonance frequencies in the plotted frequency region, and the resonance frequencies are more or less the same for all the FRFs.

The goal here is to have good fits of the form (7) for the collocated FRFs $G_{v_{p1}v_1}$ and $G_{v_{p2}v_2}$, and good fits of the form (2) for all the other FRFs. It is known (see [30] and [31]) that the beam in consideration has a multivariable state-space model of the form

$$\dot{x}(t)=Ax(t)+B_ww(t)+B_vV(t) \tag{21}$$
$$y_{\rm tip}=C_yx(t)+D_{yw}w(t)+D_{yv}V(t) \tag{22}$$
$$V_p(t)=C_vx(t)+D_{vw}w(t)+D_{vv}V(t) \tag{23}$$

where

$$A=\begin{bmatrix}0 & 1 & & 0 & 0\\ -\omega_1^2 & -2\zeta_1\omega_1 & & 0 & 0\\ & & \ddots & & \\ 0 & 0 & & 0 & 1\\ 0 & 0 & & -\omega_N^2 & -2\zeta_N\omega_N\end{bmatrix} \tag{24}$$

$$B=\begin{bmatrix}B_w & B_{v_1} & B_{v_2}\end{bmatrix}=\begin{bmatrix}0 & 0 & 0\\ \beta_1 & \Psi_1^{v_1} & \Psi_1^{v_2}\\ \vdots & \vdots & \vdots\\ 0 & 0 & 0\\ \beta_N & \Psi_N^{v_1} & \Psi_N^{v_2}\end{bmatrix} \tag{25}$$

$$\tag{26}$$

and

$$C=\begin{bmatrix}C_y\\ C_{v_1}\\ Cv_2\end{bmatrix}=\begin{bmatrix}\gamma_1 & 0 & \dots & \gamma_N & 0\\ \Psi_1^{v_1} & 0 & \dots & \Psi_N^{v_1} & 0\\ \Psi_1^{v_2} & 0 & \dots & \Psi_N^{v_2} & 0\end{bmatrix} \tag{27}$$

$$V(t)=\begin{bmatrix}v_1 & v_2\end{bmatrix}' \tag{28}$$
$$V_p(t)=\begin{bmatrix}v_{p1} & v_{p2}\end{bmatrix}'. \tag{29}$$

The terms D_{yw}, D_{vw}, D_{yv}, and D_{vv} are matrices of appropriate dimensions. Furthermore, all state-space matrices (24)–(29) are

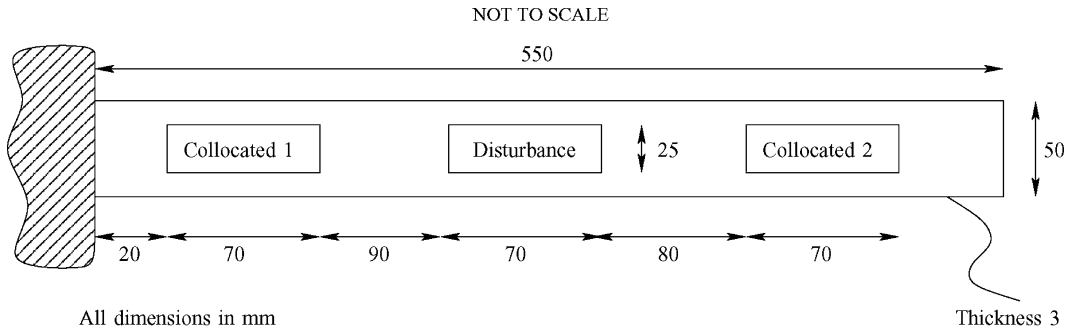

Fig. 4. Beam setup and dimensions.

TABLE I
BEAM PROPERTIES

Length, L	$550\ mm$
Thickness, h	$3\ mm$
Width, W	$50\ mm$
Density, ρ	$2.77 \times 10^3\ kg/m^3$
Young's Mod., E	$7.00 \times 10^{10}\ N/m^2$

TABLE II
PIC 151 CERAMIC PROPERTIES

Length, L_{pz}	$50\ mm$
Thickness, h_{pz}	$0.25\ mm$
Width, W_{pz}	$25\ mm$
Charge Constant, d_{31}	$-210 \times 10^{-12}\ m/V$
Voltage Constant, g_{31}	$-11.5 \times 10^{-3}\ Vm/N$
Coupling Coefficient, k_{31}	0.34
Capacitance, C_p^S	$115\ nF$

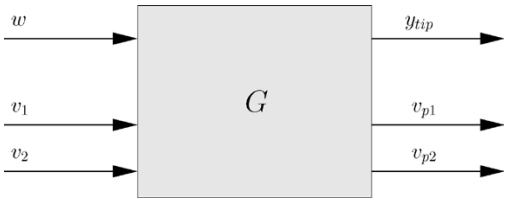

Fig. 5. Augmented MIMO plant.

assumed to be real valued. This amounts to the assumption that mode shapes of the system are real-valued functions.

Using Laplace transforms, it can be verified that (21)–(23) enforce the structure (7) on the collocated FRFs $G_{v_{p1}v_1}$ and $G_{v_{p2}v_2}$, and the structure (2) on the other noncollocated FRFs. The model structure (21)–(23) also forces all the FRFs to have the same set of poles.

Note that the given FRF data has only three resonance frequencies (see Fig. 6). In other words, the given FRF data takes into account only the first three modes of vibrations. The other higher order modes have been discarded (or not taken into account) as they are beyond the frequency regions of interest. Since the given data includes only three modes, it suffices to set $N = 3$, or consider a third-order model of the form (21)–(23). A standard method to determine the model parameters $\{\Psi_k^{v_1}, \Psi_k^{v_2}, \beta_k, \gamma_k, \omega_k, \zeta_k\}_{k=1}^N$ and the feed-through

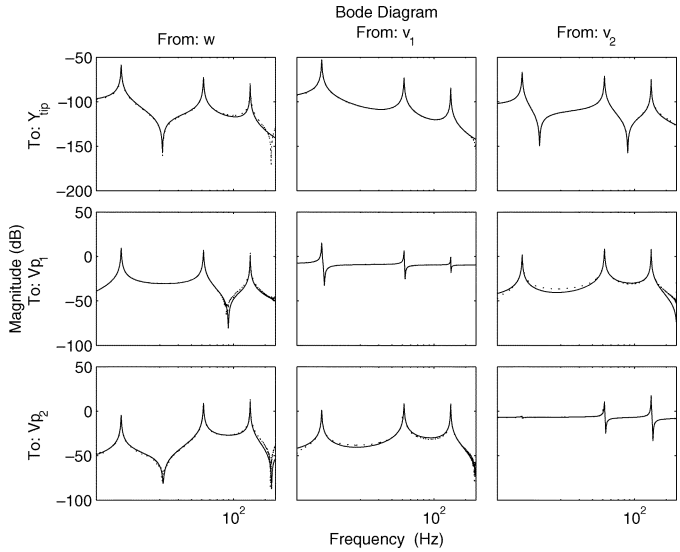

Fig. 6. (Solid) Identified model with (dotted) measured data.

terms D_{yw}, D_{yv}, D_{vw}, and D_{vv} is to choose them as the minimizers of the cost function

$$\mathcal{M} = \sum_{i,j=1}^{3} \sum_{k=1}^{M} \left| \frac{G_{ij}^N(\mathrm{i}\omega_k) - G_{ij}(\mathrm{i}\omega_k)}{G_{ij}(\mathrm{i}\omega_k)} \right|^2 \tag{30}$$

where $G_{ij}^N(\mathrm{i}\omega)$ are the FRFs corresponding to the multivariable state space model (21)–(23) and ω_k denotes the frequency points where the nonparametric FRFs $G_{ij}(\mathrm{i}\omega)$ are measured.

Minimizing the cost function $\mathcal{M}$ (30) involves using a computationally complex nonlinear search. Due to the enormity in the number of parameters to be estimated, the cost function $\mathcal{M}$ may have numerous local minima. Therefore, a poor initial guess for the parameters $\{\Psi_k^{v_1}, \Psi_k^{v_2}, \beta_k, \gamma_k, \omega_k, \zeta_k\}_{k=1}^N$, D_{yw}, D_{yv}, D_{vw} and D_{vv} (i.e., parameter values which give poor fits for the FRF data), the nonlinear search may land in a local minima which also gives a poor fit for the FRF data. An initialization which in itself gives a decent fit to the FRF data would lead the nonlinear search to the parameter values that give a good fit for the FRF data. Though such an initialization seems to be too much of an asking, it is still possible. One approach to get such initial values is to fit the nonparametric data first using subspace methods [32]. Using subspace methods one can obtain a multivariable state space model, of the same dimensions as (21)–(23), for the FRFs $G_{ij}(\mathrm{i}\omega)$. Even though subspace

methods are essentially black box methods, not conforming to any particular model structure, as the cantilever beam is known to posses a model of the form (21)–(23), the subspace fit would also resemble the models (21)–(23) to a large extent. From the subspace fit, one can then extract good initial estimates for parameters $\{\Psi_k^{v_1}, \Psi_k^{v_2}, \beta_k, \gamma_k, \omega_k, \zeta_k\}_{k=1}^{N}$, D_{yw}, D_{yv}, D_{vw}, and D_{vv}. Details on using subspace methods have not been presented here as it is very long and laborious. Interested readers are referred to [31] or [32].

In Fig. 6, the parametric model of the form (21)–(23) estimated from the nonparametric FRF data is plotted along with the measured data. It is apparent from the plots that the estimated parametric model gives a good fit for the nonparametric data. Also, as evident from subplots [2,2] and [3,3] of Fig. 6, the collocated transfer function of the system includes a nonzero feed-through term. This term cannot be removed from the model without introducing significant perturbations in the dc content of the system and substantial displacement of open-loop zeros. Hence, the need for a PPF controller that can guarantee closed-loop stability in presence of this nonzero feed-through term. Section VII explains how such a controller may be designed.

VII. PPF Controller Design

The tip displacement $y_{\rm tip}$ of the beam gives a measure of the amplitude of vibrations in the beam. As w represents disturbance, the FRF $G_{y_{\rm tip}w}(\mathrm{i}\omega) = Y_{\rm tip}(\mathrm{i}\omega)/W(\mathrm{i}\omega)$ is a good indicator of the effect of noise on the beam. A well-damped FRF $G_{y_{\rm tip}w}(\mathrm{i}\omega)$ would imply a well damped system. Hence, here, a controller is designed such that the closed-loop FRF $G_{Cl,yw}(\mathrm{i}\omega)$ corresponding to the input w and output $y_{\rm tip}$ is well damped. Alternatively stated, a controller is designed such that the poles of the closed-loop FRF $G_{Cl,yw}(\mathrm{i}\omega)$ are well inside the left half plane.

The PPF controller to be designed is a two-input two-output multivariable controller, which forms a feedback loop connecting the outputs $V_p(t) = \begin{bmatrix} v_{p1} & v_{p2} \end{bmatrix}'$ to the inputs $V(t) = \begin{bmatrix} v_1 & v_2 \end{bmatrix}'$ of the system. Sticking to the notations in Section IV, the PPF controller to be designed is of the form

$$\dot{\tilde{x}}(t) = \tilde{A}\tilde{x}(t) + \tilde{\Gamma} V_p(t) \tag{31}$$

$$V(t) = \hat{\Gamma}\tilde{x}(t) \tag{32}$$

where

$$\tilde{A} = \begin{bmatrix} 0 & 1 & & 0 & 0 \\ -\tilde{\omega}_1^2 & -2\delta_1\tilde{\omega}_1 & & 0 & 0 \\ & & \ddots & & \\ 0 & 0 & & 0 & 1 \\ 0 & 0 & & -\tilde{\omega}_3^2 & -2\delta_3\tilde{\omega}_3 \end{bmatrix} \tag{33}$$

and

$$\tilde{\Gamma} = \begin{bmatrix} 0 & 0 \\ \Gamma_1^{v_{p1}} & \Gamma_1^{v_{p2}} \\ \vdots & \vdots \\ 0 & 0 \\ \Gamma_3^{v_{p1}} & \Gamma_3^{v_{p2}} \end{bmatrix} \tag{34}$$

and

$$\hat{\Gamma} = \begin{bmatrix} \Gamma_1^{v_{p1}} & 0 & \Gamma_2^{v_{p1}} & 0 & \Gamma_3^{v_{p1}} \\ \Gamma_1^{v_{p2}} & 0 & \Gamma_2^{v_{p2}} & 0 & \Gamma_3^{v_{p2}} \end{bmatrix}. \tag{35}$$

Note that (31)–(32) is (14)–(15) written in first-order from with $\tilde{N} = 3$.

Using (31)–(32) in (21)–(23), the closed-loop system can be written in the form

$$\dot{X} = \bar{A}(\tilde{\Omega}, \Delta, \Gamma)X + \bar{B}_w w(t) \tag{36}$$

$$y_{\rm tip} = \bar{C}(\Gamma)X + \bar{D}_{yw} w(t) \tag{37}$$

where $X = \begin{bmatrix} x' & \tilde{x}' \end{bmatrix}'$ and

$$\Gamma = \begin{bmatrix} \Gamma_1^{v_{p1}} & \Gamma_2^{v_{p1}} & \Gamma_3^{v_{p1}} \\ \Gamma_1^{v_{p2}} & \Gamma_2^{v_{p2}} & \Gamma_3^{v_{p2}} \end{bmatrix}. \tag{38}$$

Derivations of the expressions for $\bar{A}(\tilde{\Omega}, \Delta, \Gamma)$, $\bar{B}$, $\bar{C}$, and $\bar{D}_{yw}$ from (31)–(32) and (21)–(23) involve standard (and straightforward) calculations and, hence, are omitted here.

The FRF $G_{Cl,yw}(\mathrm{i}\omega)$ corresponding to the closed-loop system (36)–(37) is the one that is to be damped by appropriately choosing $\tilde{\Omega}$, Δ, and Γ. A sufficiency condition for the stability of the closed loop (36)–(37) is provided by Lemma 1 in Section IV. Lemma 1 states that for the closed-loop system $G_{Cl,yw}(\mathrm{i}\omega)$ to be stable the LMI condition (19) has to be satisfied. Hence, the PPF controller design problem can be posed as a constrained optimization problem

$$\min_{\tilde{\Omega}, \Delta, \Gamma} \| G_{Cl,yw}(\mathrm{i}\omega) \| \tag{39}$$

subject to the constraint

$$\begin{bmatrix} \Omega^2 & -\Psi'\Gamma & 0 \\ -\Gamma'\Psi & \tilde{\Omega}^2 & \Gamma' \\ 0 & \Gamma & D^{-1} \end{bmatrix} > 0 \tag{40}$$

where

$$\Psi = \begin{bmatrix} \Psi_1^{v_1} & \Psi_2^{v_1} & \Psi_3^{v_1} \\ \Psi_1^{v_2} & \Psi_2^{v_2} & \Psi_3^{v_2} \end{bmatrix} \tag{41}$$

Ω is the 3×3 diagonal matrix with resonance frequencies of the beam as its diagonal elements, and D denotes the feed-through term D_{vv} of the model [see (23)]. The design variables Γ, Δ, and $\tilde{\Omega}$ are 2×3, 3×3, and 3×3 matrices, respectively, with Γ as defined in (38) and the matrices Δ and $\tilde{\Omega}$ being diagonal. In (39), $\| \cdot \|$ denotes a norm. Here, the H_∞ norm is considered as a performance measure for the controller design. A H_2 optimal PPF controller has also been designed and tested, but it is not reported here due to limited space.

Another approach to design the PPF controller would be to place the poles $\{P_k^c\}^{4N}$ of $G_{Cl,yw}(s)$ in a desired region in the left half plane. One way to design such a controller is to choose (Ω, Δ, Γ) such that

$$V = \alpha \sum_{k=1}^{4N} \mid P_k^d - Re(P_k^c) \mid^2 + \beta \sum_{i=2,\ i\ \text{even}}^{4N} \mid P_k^c - P_{k-1}^c \mid^2 \tag{42}$$

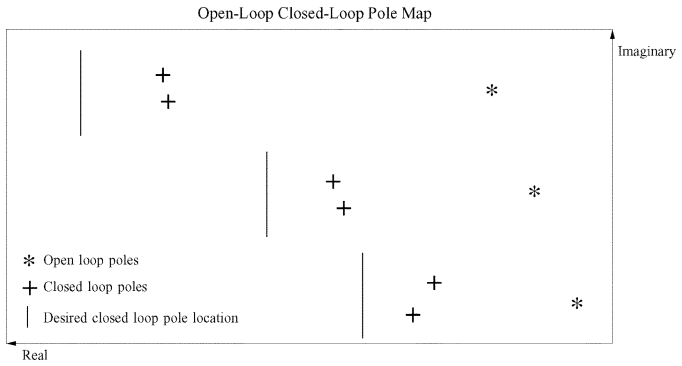

Fig. 7. Pole optimization procedure.

is minimal under the constraint (40). In (42), $\left\{P_k^d\right\}^{4N}$ denotes a set of prespecified negative real numbers, $Re(\cdot)$ denotes the real part of a complex number, and α and β are positive scalars. The first term in the right hand side of the cost function V, (42), tries to bring the real part of the closed-loop poles $\{P_k^c\}^{4N}$ close to the set of prespecified real values $\left\{P_k^d\right\}^{4N}$ in the left half plane. The second term keeps the pair of closed poles that correspond to the same open-loop pole close to each other (see Fig. 7).

As in the case of identification, both optimization problems (39) and (42) involve using a nonlinear search, which needs to be initialized amicably. One way to initialize the nonlinear search would be to solve the LMI (40) using well-known LMI solvers like SeDuMi, or Matlab LMI tool box, to obtain a feasible solution. Although such an initial condition would be valid, its use may result in a controller gain $\| \Gamma\Gamma' \|$, which is too large. A prohibitively large controller gain may result in implementation difficulties. A simple way to obtain initial values is to solve for Γ by solving the LMI (40) for certain fixed values of $\tilde{\Omega}$ and Δ. Past research (see [7], [33], and [34]) and experience with PPF controllers suggest that good PPF designs have their resonance frequencies $\tilde{\Omega}$ close to the system resonance frequencies Ω. Taking this cue, we let

$$\tilde{\Omega} = \kappa\Omega \tag{43}$$

$$\Delta = \frac{\eta}{\kappa} \tag{44}$$

where κ is a scalar reasonably close to one (for example, $\kappa = \sqrt{2}$), as our initial guesses for $\tilde{\Omega}$ and Δ. Using the initial values (43) and (44), a meaningful initial guess for Γ can be obtained in the following fashion: Let $\Psi_\perp^{v_1}$ and $\Psi_\perp^{v_2}$ denote vectors orthonormal to $\Psi^1 = \begin{bmatrix}\Psi_1^{v_1} & \Psi_1^{v_2}\end{bmatrix}'$ and $\Psi^2 = \begin{bmatrix}\Psi_2^{v_1} & \Psi_2^{v_2}\end{bmatrix}'$ [see (41)]. Note that, due to the linear independence of Ψ^1 and Ψ^2 (which is assumed), there exists C_1 and C_2 such that $\Psi^3 = \begin{bmatrix}\Psi_3^{v_1} & \Psi_3^{v_2}\end{bmatrix}'$ is equal to $C_1\Psi^1 + C_2\Psi^2$. Let $\tilde{\Gamma}_C = \begin{bmatrix}\alpha_1\Psi_\perp^1 & \alpha_2\Psi_\perp^2 & 0\end{bmatrix}$, where α_1 and α_2 are real-valued parameters, denote a candidate Γ for the initial value. It is easy to note that

$$\Psi'\Gamma_C = \begin{bmatrix}\alpha_1 & 0 & 0\\ 0 & \alpha_2 & 0\\ C_1\alpha_1 & C_2\alpha_2 & 0\end{bmatrix}. \tag{45}$$

Since the feed-through term D_{vv} is, in general, very small, we drop the quadratic term $\Gamma' D\Gamma$ in (11) and approximate it by

$$\Omega^2 - \Psi'\Gamma_C\tilde{\Omega}^{-2}\Gamma_C'\Psi > 0. \tag{46}$$

Due to the chosen structure of Γ_C, (46) can be further simplified to

$$\Omega^2\tilde{\Omega}^2 > M'M \tag{47}$$

where

$$M = \begin{bmatrix}\alpha_1 & 0 & 0\\ 0 & \alpha_2 & 0\\ C_1\alpha_1\frac{\tilde{\Omega}_3}{\tilde{\Omega}_1} & C_2\alpha_2\frac{\tilde{\Omega}_3}{\tilde{\Omega}_2} & 0\end{bmatrix}. \tag{48}$$

Note that the right-hand side of (47) is a constant diagonal matrix; therefore, choosing α_1 and α_2 such that the bound (47) is satisfied would give an initial guess for Γ_C. However, it must be stressed that the approximation introduced in (46) could fail for large values of α_1 and α_2. Hence, it is worth checking if the LMI (11) is satisfied for the chosen initial guesses.

A. Results of Pole Placement Controller Design

Schematics of the experimental setup used to implement the pole optimized PPF controller, and all subsequent controllers, is illustrated in Fig. 8. The controller was designed, and simulations were performed, in a MATLAB/SIMULINK environment. The controller was then downloaded onto a dSPACE DS-1103 rapid prototyping system. The sampling frequency of the DSP system was set to 20 kHz, and low-pass antialiasing and reconstruction filters with cutoff frequencies of 10 kHz were added to the system as shown in Fig. 8. Voltages induced in the two piezoelectric sensors were measured through high-input impedance buffer circuits, to reduce the low-frequency distortions caused by the finite impedance of the measurement device.

To determine a controller, the desired real parts of closed-loop poles in (42) were placed at -8, -66, and -120, respectively. The real parts of the actual closed-loop poles were found to be -9.7494, -60.8264, and -105.9135, respectively.

To evaluate the damping introduced in the system due to the PPF controller, both the open-loop and the closed-loop FRFs $G_{y_{\rm tip}w}(\mathrm{i}\omega)$ and $G_{Cl,y_{\rm tip}w}(\mathrm{i}\omega)$ are plotted in Figs. 10 and 11. In Fig. 10, simulated values of $G_{y_{\rm tip}w}(\mathrm{i}\omega)$ and $G_{Cl,y_{\rm tip}w}(\mathrm{i}\omega)$ are plotted, i.e., $G_{y_{\rm tip}w}(\mathrm{i}\omega)$ obtained from the model (21)–(23) and $G_{Cl,y_{\rm tip}w}(\mathrm{i}\omega)$ obtained from (36) and (37) with the parameters $\tilde{\Omega}$, Δ, and Γ set to their optimal values. In Fig. 11, experimentally determined $G_{y_{\rm tip}w}(\mathrm{i}\omega)$ and $G_{Cl,y_{\rm tip}w}(\mathrm{i}\omega)$ are plotted. Experimentally determined FRFs refer to the case where the piezoelectric patch corresponding disturbance input w in the cantilever beam setup is driven by a chirp signal and the corresponding output $y_{\rm tip}$ is recorded for both the closed- and the open-loop systems. The FRFs $G_{y_{\rm tip}w}(\mathrm{i}\omega)$ and $G_{Cl,y_{\rm tip}w}(\mathrm{i}\omega)$ are then calculated from the recorded input–output data, as done in the nonparametric identification. The simulation plots and the experimental plots are fairly similar, with the differences being not too noticeable, thus validating the use of the model (21)–(23) for the beam. The plots also suggest a satisfactory damping in the magnitude of the closed-loop FRF $G_{Cl,y_{\rm tip}w}(\mathrm{i}\omega)$ at the resonance frequencies.

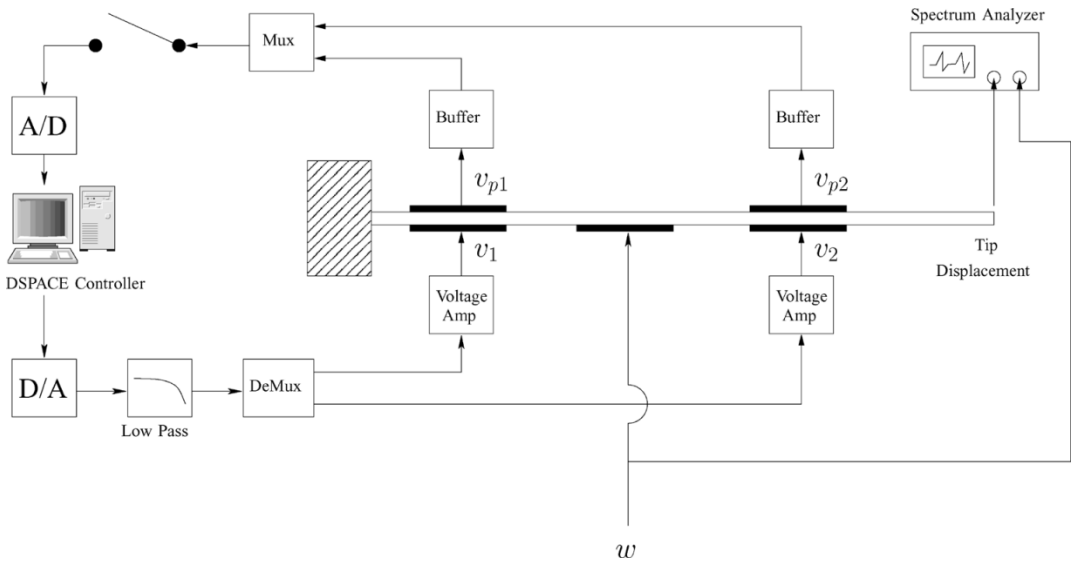

Fig. 8. Schematics of the experimental setup.

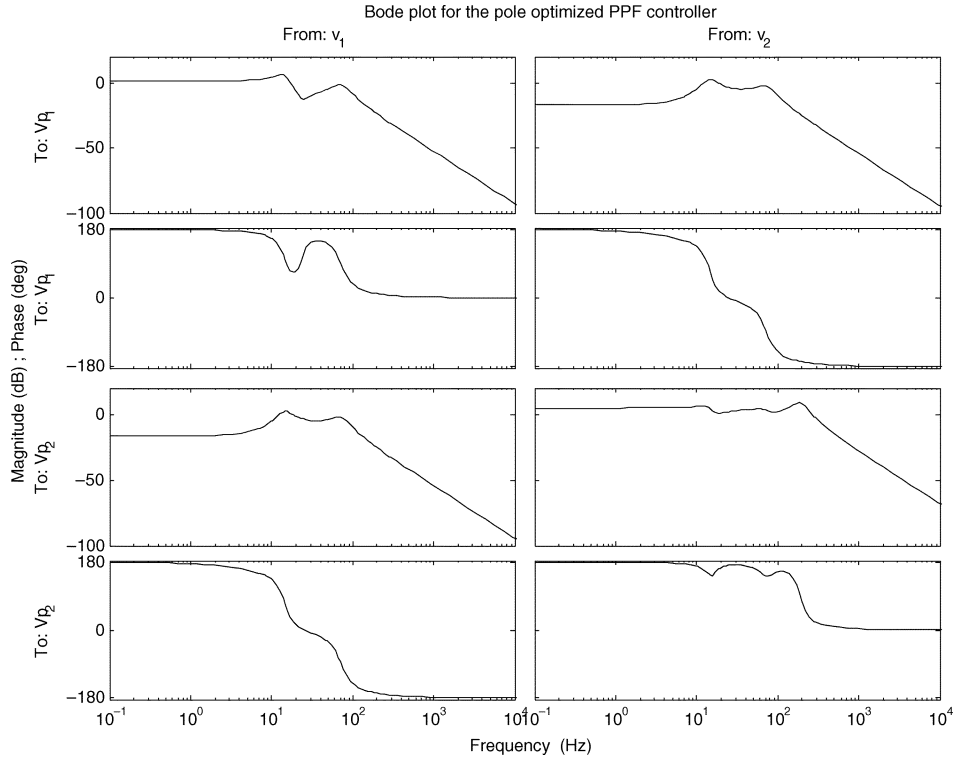

Fig. 9. PPF controller using the pole optimization.

In Fig. 12, the open-loop poles and the closed-loop pole are plotted. It is evident that $G_{Cl,y_{\rm tip}w}(\mathrm{i}\omega)$ is much better damped.

In practice, due to wear and tear and also due to other factors, such as surrounding temperature, etc., the material properties of the structure and the piezoelectric patches tend to change. This leads to shifts in the resonance frequencies of the beam. A good controller design must be robust enough to provide good damping even under the changed circumstances. In order to check the robustness of the PPF design, here, artificial shifts in the resonance frequencies of the beam were brought about by adding an extra mass at the free end of the beam. In Fig. 13, the measured open-loop and the closed-loop FRFs $G_{y_{\rm tip}w}(\mathrm{i}\omega)$ and $G_{Cl,y_{\rm tip}w}(\mathrm{i}\omega)$ for the loaded system are plotted. It must be stressed that the PPF controller used in the closed-loop system is the same PPF controller that was used for the unloaded cantilever beam. The plots suggest that the PPF controller designed using pole optimization is robust with respect to shifts in the resonance frequencies.

Finally, to illustrate controller performance in time domain, a pulse-shaped disturbance voltage was applied to the disturbance piezoelectric patch. The resulting tip displacements in open- and closed-loop were recorded for the beam with and without the tip mass. These time-domain results are plotted in Fig. 14 and

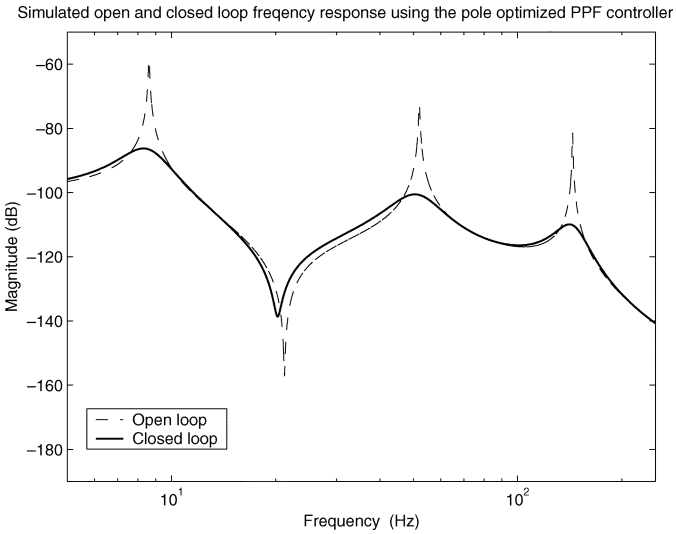

Fig. 10. Simulated open- and closed-loop frequency response using the pole optimization.

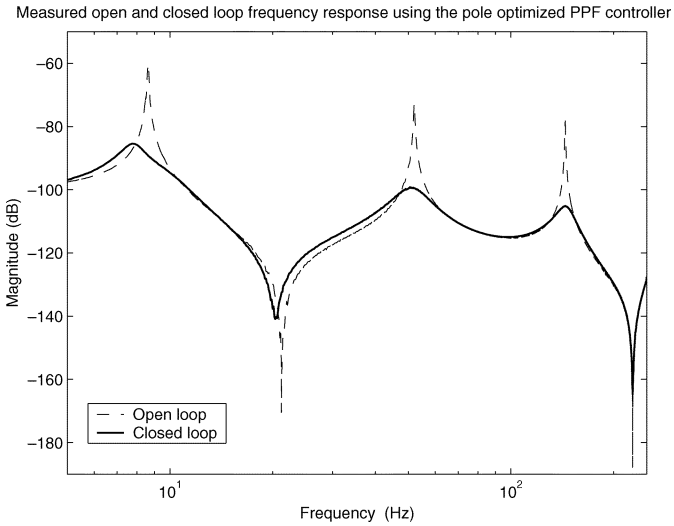

Fig. 11. Measured open- and closed-loop frequency response using the pole optimization.

clearly demonstrate the effectiveness of the controller in terms of disturbance rejection and its relative immunity to uncertainty in the structural dynamics of the system.

B. H_∞ PPF Controller

Finally, this section is concluded with the results of using H_∞ optimized PPF controller. The FRF of the H_∞ optimized PPF controller is plotted in Fig. 15. As in the previous case, the PPF controller designed by minimizing the H_∞ norm also has a good rolloff in the high frequency regions. In order to limit the level of control signals applied to the two piezoelectric actuators, the exogenous output y_{tip} is augmented with weighted versions of v_1 and v_2. The weights are chosen carefully to trade off between the achievable damping and the necessary control signals. This is a standard approach [35]; hence, no more details are included here.

In Figs. 16 and 17, the closed-loop and the open-loop FRFs are plotted. The plots suggest a good damping of the closed loop due to the PPF controller. The plots also suggest good agreement between the simulated and the experimental FRFs.

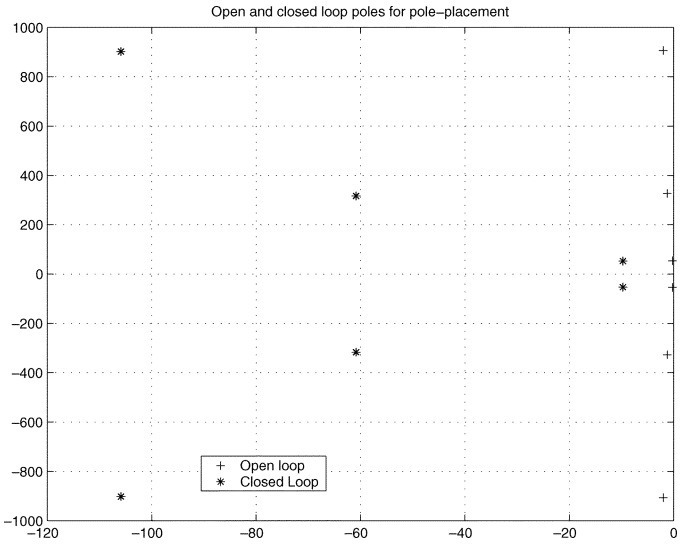

Fig. 12. Open- and closed-loop pole map for the pole placement optimization.

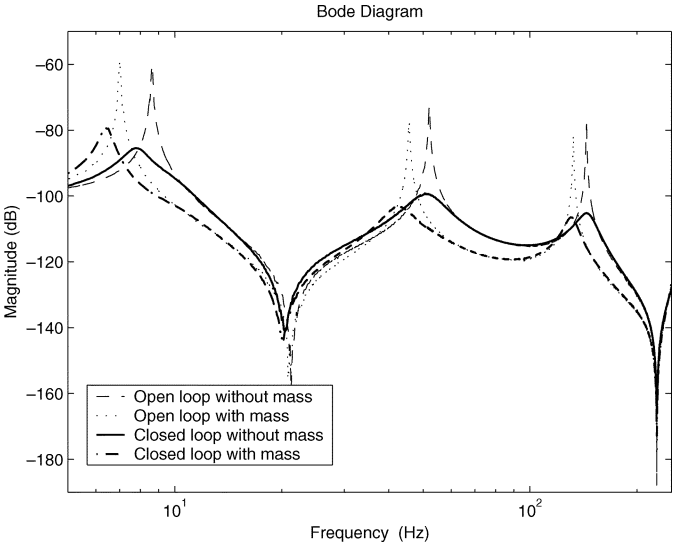

Fig. 13. Measured open- and closed-loop frequency responses using the pole optimization, with and without the mass.

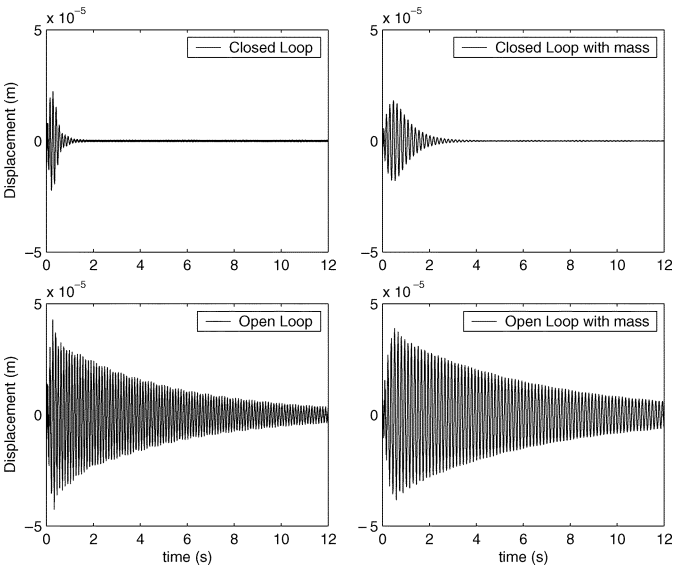

Fig. 14. Measured disturbance response using pole optimization, with and without the mass.

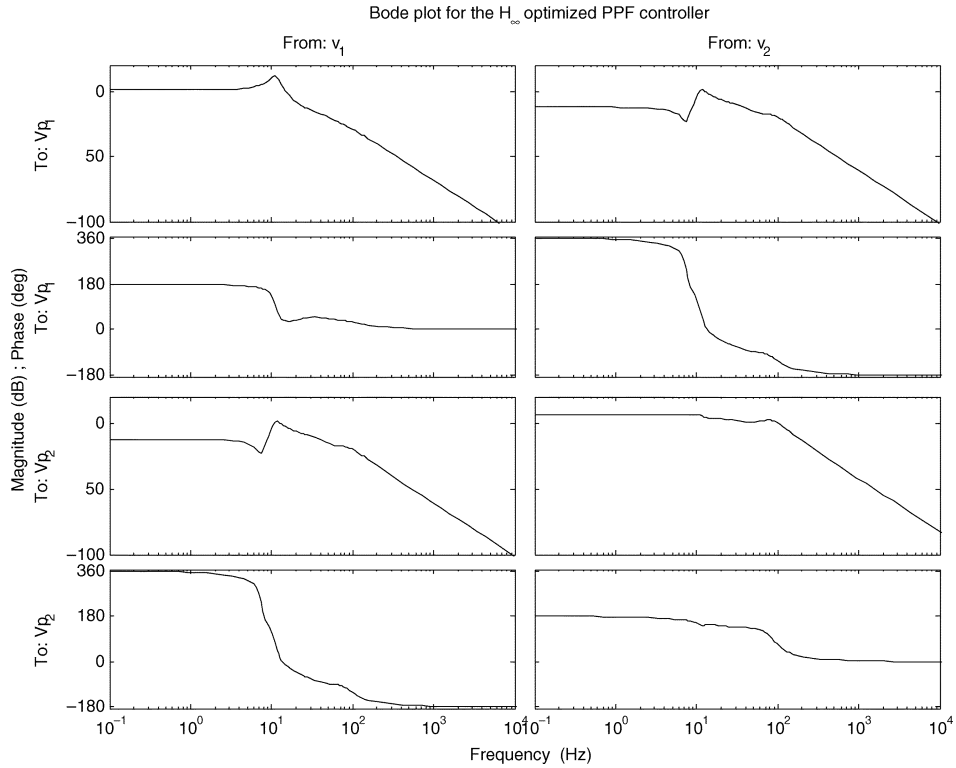

Fig. 15. PPF Controller using the $\mathcal{H}_\infty$ optimization.

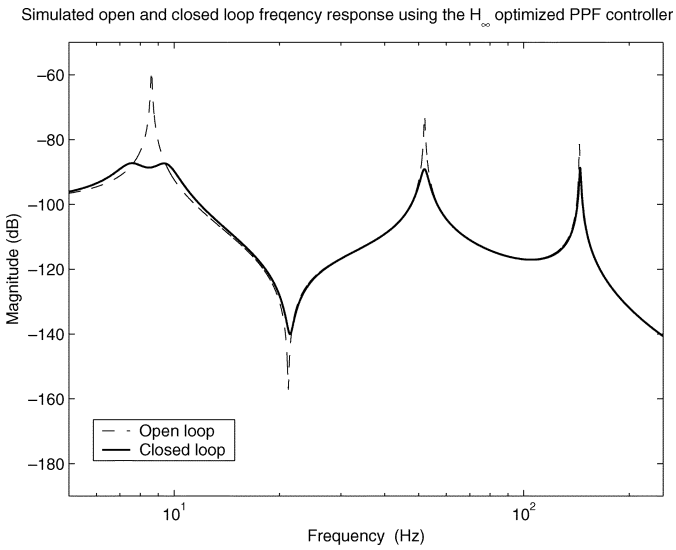

Fig. 16. Simulated open- and closed-loop frequency responses using $\mathcal{H}_\infty$ optimization.

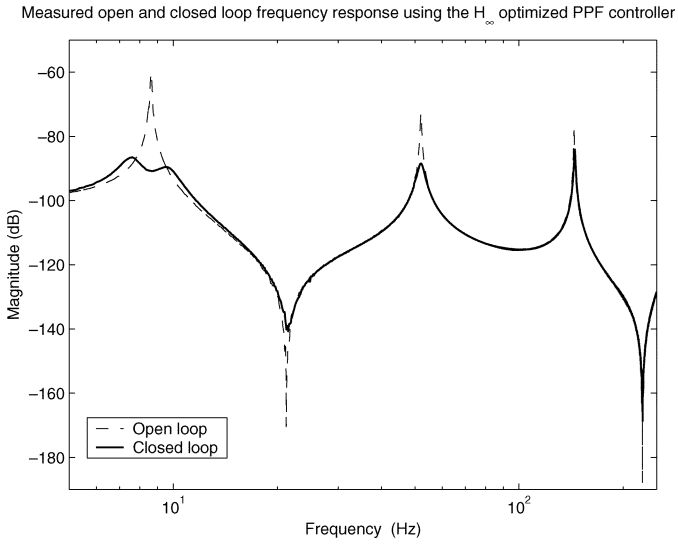

Fig. 17. Measured open- and closed-loop frequency responses using $\mathcal{H}_\infty$ optimization.

In Fig. 18, the poles of the open- and the closed-loop systems are presented. As in the earlier case the plot suggests a good deal of damping in the closed-loop system due to the PPF controller.

Robustness of the H_∞ optimized PPF controller is tested by using it on the loaded cantilever beam. The plots in Fig. 19 suggest that the H_∞ minimized PPF controller is also robust to changes in the resonance frequencies of the beam.

Finally, to observe performance of the H_∞ optimized PPF in time-domain, similar time domain tests are performed on the system. The results are illustrated in Fig. 20.

VIII. Conclusion

In this paper, we derived stability conditions for PPF controllers when the underlying structure model contains a feed-through term. PPF controllers are generally employed to damp structural vibration of systems with collocated actuators and sensors. Dynamics of such distributed parameter systems typically consist of a large number of modes. Higher frequency modes are often removed to obtain a low-order model that lends itself to standard control design tools. To ignore high-frequency dynamics in such models may add significant uncertainty to the model which may bring about a degradation in the closed-loop performance of

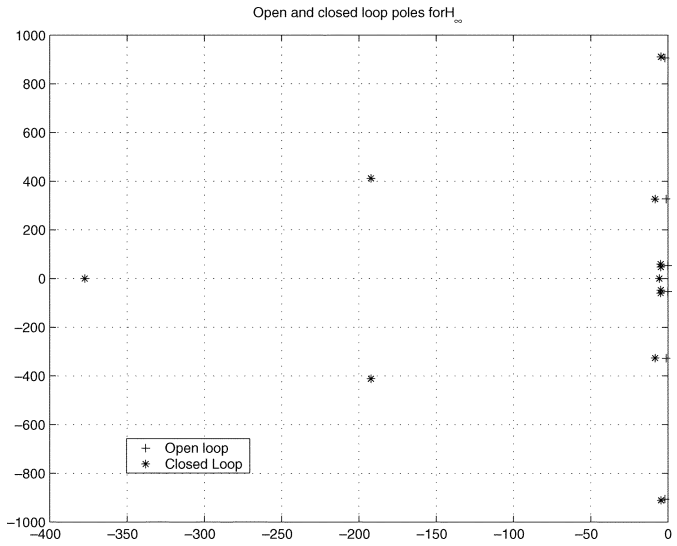

Fig. 18. Open- and closed-loop pole map for the $\mathcal{H}_\infty$ optimization.

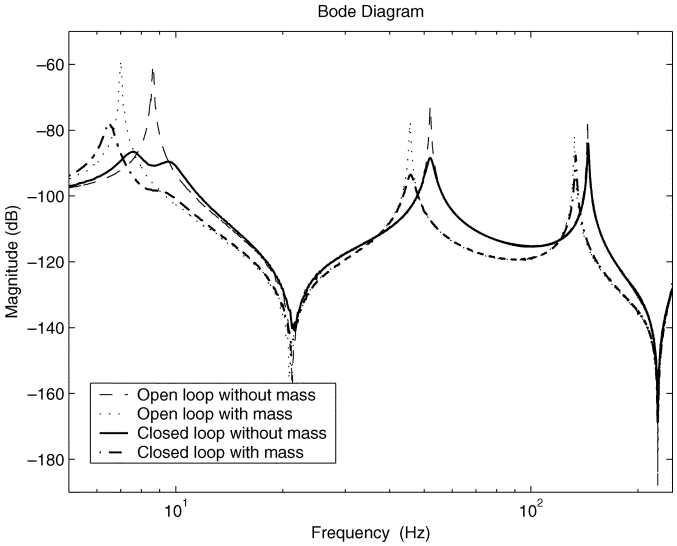

Fig. 19. Measured open- and closed-loop frequency responses using the $\mathcal{H}_\infty$ optimization, with and without the mass.

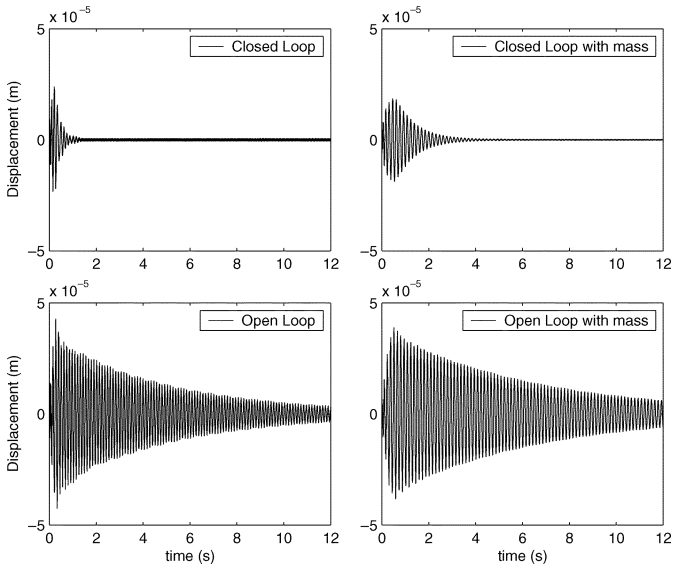

Fig. 20. Measured disturbance responses using the $\mathcal{H}_\infty$ optimization, with and without the mass.

the controller once implemented on the system. By appending a static term to the truncated model, the uncertainty within the bandwidth of interest can be substantially reduced.

We demonstrated that the class of stabilizing PPF controllers is a convex set characterized by a set of linear matrix inequalities. We also explained how an optimization problem can be setup to obtain a PPF controller which can provide sufficient damping. Two PPF controllers were designed for and implemented on an active structure consisting of two collocated piezoelectric actuator/sensor pairs. The multivariable PPF controllers were shown to add significant damping to the structure. These controllers are also surprisingly resilient toward changes in the resonance frequencies of the base structure. By adding a small mass to the structure, its resonance frequencies were shifted by over 10%. Despite this, the PPF controllers gracefully maintained closed-loop stability and performance.

Optimization procedures proposed in this paper are numerically tractable, as illustrated through several examples. The problem of PPF controller design is essentially reduced to solving a nonlinear optimization problem over a convex set. This, along with a procedure for choosing an appropriate starting point, results in PPF controllers of the kind reported in this paper. Future research in this area should investigate the possibility of obtaining a convex solution to the problem of PPF controller design.

REFERENCES

[1] M. J. Balas, "Active control of flexible systems," *J. Optim. Theory Appl.*, vol. 25, no. 3, pp. 415–436, 1978.
[2] ——, "Feedback control of flexible systems," *IEEE Trans. Autom. Contr.*, vol. AC-23, no. 4, pp. 673–679, Aug. 1978.
[3] C. W. de Silva, *Vibration Fundamentals and Practice*. Boca Raton, FL: CRC, 1999.
[4] J. Juang and M. Q. Phan, *Identification and Control of Mechanical Systems*. Cambridge, U.K.: Cambridge Univ. Press, 2001.
[5] S. O. R. Moheimani and B. J. G. Vautier, "Resonant control of structural vibration using charge-driven piezoelectric actuators," presented at the IEEE Conf. Decision and Control, 2004.
[6] C. J. Goh and T. K. Caughey, "On the stability problem caused by finite actuator dynamics in the collocated control of large space structures," *Int. J. Contr.*, vol. 41, no. 3, pp. 787–802, 1985.
[7] J. L. Fanson and T. K. Caughey, "Positive position feedback-control for large space structures," *AIAA J.*, vol. 28, no. 4, pp. 717–724, Apr. 1990.
[8] L. Meirovitch, *Elements of Vibration Analysis*, 2nd ed. Sydney, Australia: McGraw-Hill, 1986.
[9] R. L. Clark, "Accounting for out-of-bandwidth modes in the assumed modes approach: Implications on colocated output feedback control," *Trans. ASME, J. Dyn. Syst., Meas., Contr.*, vol. 119, no. 1, pp. 390–395, Mar. 1997.
[10] S. O. R. Moheimani, "Experimental verification of the corrected transfer function of a piezoelectric laminate beam," *IEEE Trans. Contr. Syst. Technol.*, vol. 8, no. 4, pp. 660–666, Jul. 2000.
[11] P. C. Hughes, "Space structure vibration modes: How many exist? Which ones are important?," *IEEE Contr. Syst. Mag.*, vol. 8, no. 1, pp. 22–28, Feb. 1987.
[12] G. D. Martin, "On the control of flexible mechanical systems," Ph.D. dissertation, Dept. Aeronaut. Astronaut., Stanford Univ., Stanford, CA, 1978.
[13] J. N. Aubrun, "Theory of control of structures by low-authority controllers," *Int. J. Contr.*, vol. 3, no. 5, pp. 444–451, 1980.
[14] A. G. Kelkar and S. M. Joshi, "Control of elastic systems via passivity-based methods," *J. Vibr. Contr.*, vol. 10, no. 11, pp. 1699–1735, Nov. 2004.
[15] ——, "Passivity-based robust control with application to benchmark active controls technology wing," *J. Guid., Contr. Dyn.*, vol. 23, no. 5, pp. 938–947, Sep.-Oct. 2000.
[16] R. L. Bisplinghoff and H. Ashley, *Principles of Aeroelasticity*. New York: Dover, 1962.

[17] S. O. R. Moheimani, "Minimizing the effect of out of bandwidth modes in truncated structure models," *Trans. ASME J. Dyn. Syst., Meas., Contr.*, vol. 122, no. 1, pp. 237–239, Mar. 2000.
[18] S. O. R. Moheimani and W. P. Heath, "Model correction for a class of spatio-temporal systems," *Automatica*, vol. 38, no. 1, pp. 147–155, Jan. 2002.
[19] M. M. Seron, J. H. Braslavsky, and G. C. Goodwin, *Fundamental Limitations in Filtering and Control*. London, U.K.: Springer, 1997.
[20] S. Boyd, L. El Ghaoui, E. Feron, and V. Balakrishnan, *Linear Matrix Inequalities in System and Control Theory*. Philadelphia, PA: SIAM, 1994.
[21] K. H. Rew, J. H. Han, and I. Lee, "Multi-modal vibration control using adaptive positive position feedback," *J. Intell. Mater. Syst. Struct.*, vol. 13, no. 1, pp. 13–22, Jan. 2002.
[22] G. Song, P. Z. Qiao, W. K. Binienda, and G. P. Zou, "Active vibration damping of composite beam using smart sensors and actuators," *J. Aerosp. Eng.*, vol. 15, no. 3, pp. 97–103, Jul. 2002.
[23] J. H. Han, J. Tani, and I. Lee, "Multi-modal vibration control of smart composite plates," *Mater. Sci. Res. Int.*, vol. 5, no. 2, pp. 122–127, Jun. 1999.
[24] L. Vaillon and C. Philippe, "Passive and active microvibration control for very high pointing accuracy space systems," *Smart Mater. Struct.*, vol. 8, no. 6, pp. 719–728, Dec. 1999.
[25] C. Choi and K. Park, "Self-sensing magnetic levitation using a lc resonant circuit," *Sens. Actuators A*, vol. 72, no. 2, pp. 169–177, Jan. 1999.
[26] M. I. Friswell, D. J. Inman, and R. W. Rietz, "Active damping of thermally induced vibrations," *J. Intell. Mater. Syst. Struct.*, vol. 8, no. 8, pp. 678–685, Aug. 1997.
[27] D. J. Leo and D. J. Inman, "Pointing control and vibration suppression of a slewing flexible frame," *J. Guid. Contr. Dyn.*, vol. 17, no. 3, pp. 529–536, 1994.
[28] S. Devasia, T. Meressi, B. Paden, and E. Bayo, "Piezoelectric actuator design for vibration suppression – Placement and sizing," *J. Guid. Contr. Dyn.*, vol. 16, no. 5, pp. 859–864, 1993.
[29] J. L. Fanson, E. H. Anderson, and D. Rapp, "Active structures for use in precision control of large optical-systems," *Opt. Eng.*, vol. 29, no. 11, Nov. 1990.
[30] S. O. R. Moheimani, D. Halim, and A. J. Fleming, *Spatial Control of Vibration: Theory and Experiments*, Singapore: World Scientific, 2003.
[31] B. J. G. Vautier, "Charge-driven piezoelectric actuators in structural vibration control applications," M.S. thesis, Dept. Elect. Eng., Univ. Newcastle, Newcastle, Australia, 2004.
[32] T. McKelvey, H. Ackay, and L. Ljung, "Subspace-based identification of infinite-dimensional multi-variable systems from frequency-response data," *IEEE Trans. Autom. Contr.*, vol. AC–41, no. 7, pp. 960–979, Jul. 1996.
[33] G. Song, S. P. Schmidt, and B. N. Agrawal, "Experimental robustness study of positive position feedback control for active vibration suppression," *J. Guid., Contr., Dyn.*, vol. 25, no. 1, pp. 179–182, 2002.
[34] J. L. Fanson and T. K. Caughey, "Positive position feedback control for large space strcture," in *Proc. 28th AIAA/ASME/ASC/AHS Structures Structural Dynamics and Materials Conf.*, Monterey, CA, 1987, pp. 588–598.
[35] K. Zhou, J. C. Doyle, and K. Glover, *Robust and Optimal Control*. Englewood Cliffs, NJ: Prentice Hall, 1996.

S. O. Reza Moheimani (S'93–M'97–SM'00) received the Ph.D. degree in electrical and electronic engineering from the University of New South Wales, Australia, in 1996.

Following a research position at the University of New South Wales, he joined the University of Newcastle, Newcastle, Australia, in 1997, where he is currently an Associate Professor with the School of Electrical Engineering and Computer Science, the Director of Laboratory for Dynamics and Control of Smart Structures, and a program leader for the ARC Centre for Complex Dynamic Systems and Control, an Australian Government Centre of Excellence. He has published two books, several edited volumes, and over 100 refereed articles in the areas of robust control and estimation, smart structures, active noise and vibration control, mechatronic systems, and nanotechnology.

Dr. Moheimani is an Associate Editor of several international journals including the IEEE TRANSACTIONS ON CONTROL SYSTEMS TECHNOLOGY and has chaired a number of international workshops and conferences.

Benjamin J. G. Vautier was born in 1978. He received the B.Eng. degree in mechanical engineering from the University of Western Australia, Perth, in 2001, and the M.Eng. degree in electrical engineering from the University of Newcastle, Newcastle, Australia, in 2004.

His research interests include understanding and compensating for hysteresis in piezoelectric transducers and the design of multivariable controllers in structural vibration control applications.

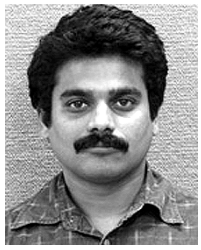

Bharath Bhikkaji received the Ph.D. degree in signal processing from Uppsala University, Uppsala, Sweden, in 2004.

Currently, he is a Research Associate with the Smart Structures Laboratory, School of Electrical Engineering and Computer Science, University of Newcastle, Newcastle, Australia. His research interests include vibration control and robust damping of highly resonant structures.